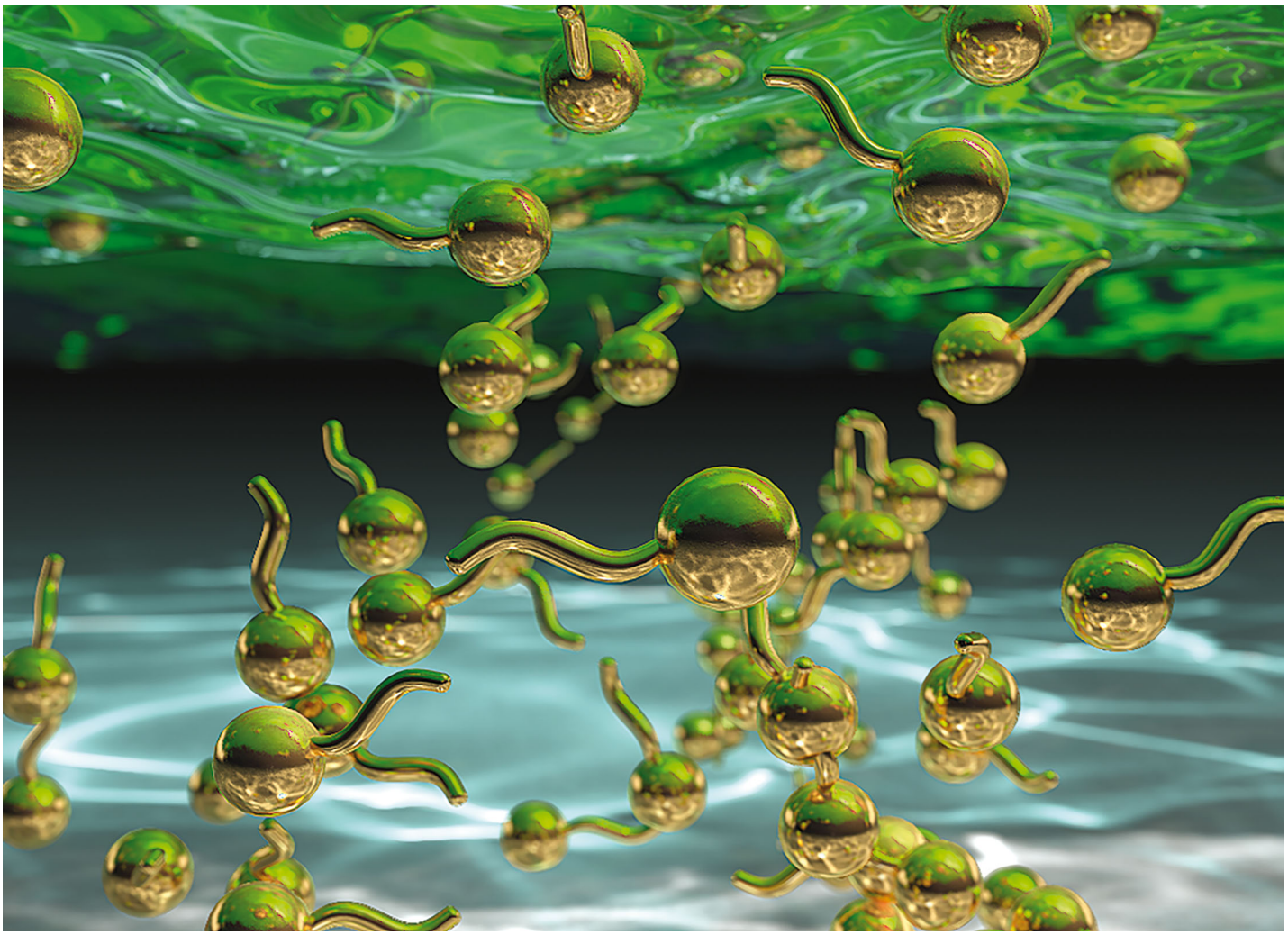

Showcasing research from Professor Pedro Camargo's laboratory, Department of Chemistry, University of Helsinki, Finland.

A mechano-colloidal approach for the controlled synthesis of metal nanoparticles

A method combining mechanochemical and colloidal synthesis was developed to produce Au nanotadpoles at room temperature. It comprises the generation of nanoparticle seeds by ball-milling followed by a seeded-growth step in water to yield the target morphology.

As featured in:

See Pedro H. C. Camargo *et al.*, *Chem. Commun.*, 2019, **55**, 14267.

ROYAL SOCIETY OF CHEMISTRY | Celebrating IYPT 2019

rsc.li/chemcomm

Registered charity number: 207890

ChemComm

COMMUNICATION

View Article Online
View Journal | View Issue

Cite this: *Chem. Commun.*, 2019, **55**, 14267

Received 10th August 2019,
Accepted 21st October 2019

DOI: 10.1039/c9cc06199a

rsc.li/chemcomm

A mechano-colloidal approach for the controlled synthesis of metal nanoparticles†

Paulo F. M. de Oliveira,[a] Jhon Quiroz,[ab] Daniela C. de Oliveira[c] and Pedro H. C. Camargo *[ab]

A mechano-colloidal approach was developed to produce Au nanotadpoles. It comprises the generation of seeds by ball-milling from a solid mixture containing a precursor, reductant, and capping agent, followed by the dispersion of this mixture in water leading to seeded-growth to generate the target nanoparticle morphology.

The size and shape controlled synthesis of metal nanoparticles (NPs) has emerged as an efficient strategy not only to the optimization of desired properties but also to unravel structure-performance relationships.[1] Solution-phase methods based on the reduction or decomposition of precursors to generate the desired growth species have been successful for the synthesis of metal NPs with controlled physical and chemical features.[2] However, the synthesis of truly controlled metal NPs can require relatively high temperatures and it is limited in terms of versatility.[3] Moreover, there is still a need for synthetic approaches that are relatively simple, robust, and scalable for generating controlled metal nanoparticles.

Mechanochemical methods, such as ball-milling, have also been employed for the synthesis of metal NPs and other nanostructures.[4] Ball milling procedures carried out under ambient conditions have enabled the simple and reproducible solvent-free synthesis of NPs.[4a–f] Scalability, stability and the possibility to handle different chemistries (*e.g.*, solubility) can be highlighted as mechanochemistry advantages.[4c] Although controlled NPs could be achieved in some cases,[4c,e] shape control can be very challenging due to the slow molecular and ion diffusion as well as different reactivities of precursors in the solid relative to liquid phases.[5]

In order to bridge this gap, we propose herein a mechano-colloidal approach in which the combination of both methods allows a nice and unusual shape control. This method allows for marrying the attractive features of both mechanochemical and colloidal synthesis while circumventing their individual limitations. The principles of the approach are depicted in Fig. 1 and consist of two main steps. In the first, mechanochemistry is employed to generate the metal NPs seeds, at room temperature, from a solid mixture containing a metal precursor (M^{x+}), a reducing agent (R_A), and a capping agent (C_A). At the end of this stage, a mixture containing the NPs seeds, the unreacted metal precursor (from its partial reduction or decomposition), and the reducing and capping agents must be present. Then, in the second step, this mixture is dispersed in water (or another solvent), in which a solution phase seeded growth occurs. This leads to an efficient separation between nucleation and growth in the second step, offering better control over the size distribution and morphology evolution (which is often a limitation for shape control by mechanochemical synthesis).[6] Moreover, the first mechanochemical step confers simplicity, scalability, and robustness to the synthesis (which is often challenging in colloidal methods). By employing the synthesis of gold (Au) NPs as a proof-of-concept example, we demonstrate that this mechano-colloidal approach can lead to the synthesis of Au nanotadpoles at room temperature by employing AuCl, sodium citrate, and polyvinylpyrrolidone (PVP) as starting materials.

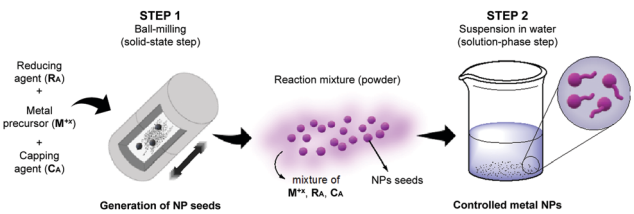

Fig. 1 Mechano-colloidal synthesis of metal NPs. In the first step, ball-milling is employed to generate the metal NPs seeds, at room temperature, from a mixture containing a metal precursor (M^{x+}), a reducing agent (R_A), and a capping agent (C_A). Then, in the second step, this mixture, that also must contain the unreacted metal precursor, can be dispersed in water or another solvent. In this second step, a solution-phase seeded growth step takes place, leading to the formation of the desired NPs.

[a] *Departamento de Química Fundamental, Instituto de Química, Universidade de São Paulo, São Paulo, SP, Brazil*
[b] *Department of Chemistry, University of Helsinki, A.I. Virtasen aukio 1, Helsinki, Finland. E-mail: pedro.camargo@helsinki.fi*
[c] *Centro Nacional de Pesquisa em Energia e Materiais, Laboratorio Nacional de Luz Síncrotron, 13083-970, Campinas, SP, Brazil*

† Electronic supplementary information (ESI) available: Experimental details, TEM and control experiments. See DOI: 10.1039/c9cc06199a

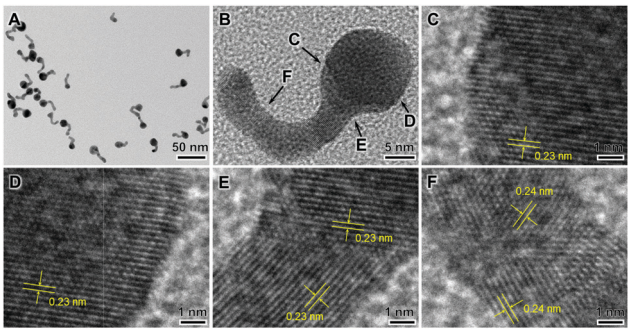

Fig. 2 HRTEM (A–F) images of Au nanotadpoles prepared by a mechano-colloidal approach that consisted in ball-milling a mixture of AuCl, sodium citrate, and PVP during 120 min at room temperature and subsequently dispersed in water for 30 min. (B) HRTEM image of a single Au nanotadpole. (C–F) Zoomed-in HRTEM images of different regions of the nanotadpole shown in (B). The Au : citrate and Au : PVP molar ratios corresponded to 1 : 1 and 1 : 8, respectively. The ball-to-powder mass ratio (bpr) was 95 : 1.

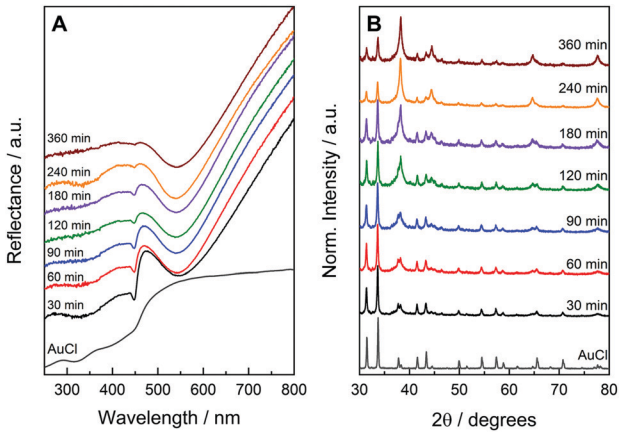

Fig. 3 UV-VIS diffusive reflectance spectra (A) and XRD patterns (B) of the solid samples containing a mixture of AuCl, citrate, and PVP recorded as a function of time during ball-milling (first step) of the mechano-colloidal synthesis. The bpr corresponded to 95 : 1. The Au : citrate and Au : PVP molar ratios were to 1 : 1 and 1 : 8, respectively. The UV-VIS spectrum and XRD pattern for AuCl is also shown for comparison (bottom traces).

Fig. 2(A–F) displays HRTEM images of a sample that was prepared by ball-milling a mixture of AuCl, sodium citrate, and PVP during 120 min at room temperature followed by dispersion in water for 30 min. Au nanotadpoles having a well-defined morphology consisting of a spherical head, with diameters ranging from 10–18 nm, and tails that were up to 22 nm in length and 5 nm in width (Fig. 2A) were detected. Fig. 2B depicts an HRTEM image for a single nanotadpole, and Fig. 2C–F shows zoomed-in images at different regions of the nanotadpole as indicated in Fig. 2B. From these images, the lattice fringes assigned to fcc Au can be clearly visualized (COD ID 1100138).[7] Moreover, it can be observed that the tails were polycrystalline and displayed undulating or bent shapes and rounded surfaces. The tail in Fig. 2B–F is composed of several domains with a single-crystal or twinned structure. These domains are connected by regions in which lattice fringes could not be detected. These morphological features indicate that the tail of the nanotadpoles is generated *via* a non-classical mechanism involving imperfect oriented attachment (coalescence of nanocrystal subunits).[8]

In order to understand the formation mechanism of the nanotadpoles, we monitored the chemical and morphological evolution of the reaction mixture as a function of time during the first ball-milling step (employing a 95 : 1 ball-to-powder ratio as well as Au : citrate and Au : PVP molar ratios corresponding to 1 : 1 and 1 : 8, respectively).[9] The UV-VIS diffusive reflectance spectra from the solid samples as a function of ball-milling time are presented in Fig. 3A. After 30 min of ball-milling, a band with a peak centered at 540 nm can be observed. This band is assigned to the dipolar LSPR mode in Au NPs, suggesting their formation after 30 min of ball milling.[10] The spectrum at this stage also presented band in 450 nm that is characteristic of AuCl (indicating the presence of both Au NPs and AuCl after 30 min of ball-milling). As the ball-milling time increased, the intensity of this band assigned to AuCl gradually decreased in agreement with the AuCl to metallic Au conversion. The AuCl band significantly decreased after 360 min of ball milling (it was almost not detectable at this stage). When we doubled the number of milling balls (the bpr was increased from 95 : 1 to 190 : 1), the AuCl band disappeared after 240 min, indicating a faster AuCl to Au conversion at higher bpr values (Fig. S1A, ESI†), as expected. Under this condition, if the Au : citrate molar ratio is increased from 1 : 1 to 1 : 4, the disappearance of the AuCl band could be observed after 120 min, indicating that a higher citrate concentration can also lead to a faster AuCl to Au conversion. This observation suggests that citrate act as an effective reducing agent in this approach (Fig. S1A, ESI†).

Fig. 3B shows XRD patterns for the solid samples under the same conditions as described in Fig. 3A. After 30 min of ball-milling, a mixture of diffraction peaks assigned to AuCl and metallic Au can be observed. The intensity of the Au peaks relative to AuCl increased as a function of time in agreement with the AuCl to Au conversion and the UV-VIS data. After 360 min of ball milling, peaks assigned to both AuCl and Au can be detected, indicating that the solid mixture still contains these two components at this stage. Similar to what was observed by UV-VIS, an increase in the bpr from 95 : 1 to 190 : 1 leads to the disappearance of the AuCl peaks after 240 min, and an increase in the Au : citrate molar ratio from 1 : 1 to 1 : 4 enables a further decrease in time for the disappearance of the AuCl peaks to 120 min, which is a result of an increased AuCl to Au conversion as a function of bpr and citrate concentration (Fig. S1B, ESI†). Fig. S2 (ESI†) shows TEM images of the Au NPs produced during the ball-milling step as a function of milling time. It can be observed that only spherical NPs were produced during the mechano-chemical step, in which the size increased with the milling time.

X-ray absorption spectroscopy (XAS) was employed in order to monitor the kinetics of the AuCl to Au (Au(I) to Au(0)) conversion during the ball-milling step of the mechano-colloidal synthesis. We recorded the X-ray absorption near edge spectra (XANES) for the samples at the Au L3 edge as a function of the ball-milling time of the reaction mixture is shown in Fig. 4A (bpr 95 : 1, Au : citrate 1 : 1). By studying both the position of the white line and the absorption profile as a function of time, the oxidation state and d-occupancy of Au can be revealed.[11] Also, quantitative

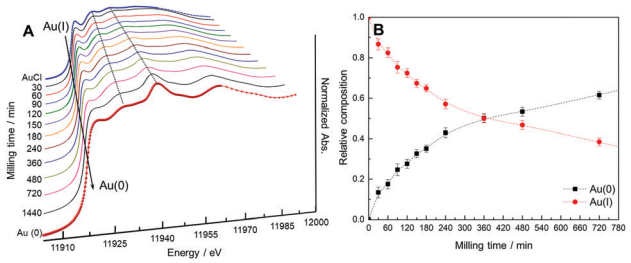

Fig. 4 (A) Normalized absorption coefficient *versus* photon energy (XANES region) for the Au L3-edge spectra of the solid samples containing a mixture of AuCl, citrate, and PVP as a function of ball-milling time during the first stage of the mechano-colloidal synthesis (bpr 95 : 1; Au : citrate and Au : PVP molar ratios corresponding to 1 : 1 and 1 : 8, respectively). The XANES spectra of the standards AuCl sample and Au(0) foil are also shown for comparison. (B) Relative composition of Au(I) and Au(0) species in the reaction mixture as a function of ball-milling time calculated by a linear combination from the XANES spectra shown in (A).

information on the nature of Au species that are present in the sample can be estimated. In this case, the Au L3 edge probes the transition of 2p electrons to unoccupied 5d states or empty density of states that have mainly d-character.[11a]

Fig. 4A shows that there is a progressive shift of the edge position and a decrease in intensity of the white line a function of the ball milling time. This is observed as we continuously transition from AuCl to Au(0) in the reaction mixture. These changes start from 30 min of ball milling and evolve up to 1440 min, in which a profile similar to the Au foil standard was obtained. This indicates the presence of only metallic Au in the final sample. This is also supported by the detected flattening of the white line. Interestingly, the XANES spectra indicate that the ball-milling step involves the reduction of Au(I) to Au(0) without the formation of any other Au species, such as Au(III).[12] We also estimated the relative composition of Au(I) to Au(0) species from the XANES spectra as a function of the ball-milling time as shown in Fig. 4B. This was achieved by a linear combination fitting using the standard spectra of AuCl and Au(0) foil.[13] Our data agree with the gradual conversion of AuCl to metallic Au, in which the total conversion was not observed up to 720 min of ball milling (longer milling times are required to achieve a complete conversion in the employed conditions). These results indicate that the reaction mixture after 120 min of ball milling contained 72% of Au(I) and 28% of Au(0).

We then studied how the variation in the ball-milling time influenced the morphology of the nanotadoples produced by the mechano-colloidal method. Fig. S3 (ESI†) shows TEM images for the nanomaterials produced by employing 30, 60, 90, and 240 min as the ball-milling time under similar conditions as described in Fig. 2 (ball milling and solution-phase steps). Nanotadpoles were detected in all cases. Because both Au(0) and AuCl are present in the reaction mixture after the ball-milling step, we would like to hypothesize that the Au NPs are generated during the ball-milling step and AuCl that remained acts as a source of Au growth species during the solution phase step that leads to the formation of the tails from the Au NPs seeds by oriented attachment (formation of nanotadpoles).[8,14] This observation is supported by the TEM images of the samples obtained by increasing the bpr to 190 : 1 and higher citrate concentration, which revealed the formation of irregular, spherical Au NPs (nanotadpoles were not observed, Fig. S4, ESI†). Under this condition, the AuCl precursor is consumed in the ball-milling step. Consequently, no AuCl is left to contribute to a solution-phase step which leads to the formation of nanotadpoles. In order to confirm the role that AuCl plays during the solution-phase step, a mixture of AuCl, citrate, and PVP was suspended in water (identical conditions for the solution-phase step that leads to the formation of the nanotadpoles). During the first hours, the AuCl remained precipitated and only after some days it was possible to see the color change and the formation of NPs. In this case, the formation of irregular Au NPs, plate-like structures, and some irregular, elongated Au nanostructures were observed (Fig. S5, ESI†). These results agree with the fact that AuCl can act as the source of Au growth species during the solution-phase step, and that oriented attachment can take place under these conditions.[8,14] It is important that the size of the Au heads in the nanotadpoles increased as a function of ball-milling time (from 8 to 11 nm as the time increased from 30 to 90 min). At longer reaction times, Au(0) growth species generated from AuCl contribute to the formation of Au NPs *via* atomic addition, leading to larger Au NPs seeds as the ball-milling time increases (Fig. S2, ESI†).

We also studied the formation of the nanotadpoles by probing the morphological evolution by TEM as a function of time during the solution-phase step as shown in Fig. 5. The initially spherical Au NPs start to present a small elongation after 5 min (Fig. 5A), which increases and leads to the formation of small tails after 15 min (Fig. 5B) and then further grow to form nanotadpoles after 30 min (Fig. 5C). These results confirm that the Au NPs seeds are formed during the first step of the mechano-colloidal approach

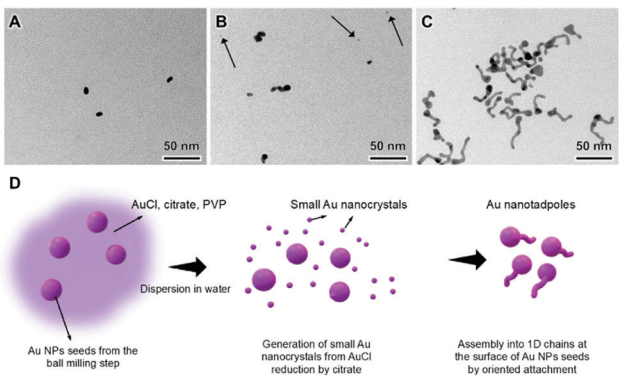

Fig. 5 (A–C) TEM images depicting the morphological evolution of the samples during the solution-phase step following ball-milling. Here, aliquots were isolated from the reaction suspension after (A) 5, (B) 15 and (C) 30 min during the solution-phase step following ball-milling (30 min of milling, bpr 95 : 1; Au : citrate and Au : PVP molar ratios corresponding to 1 : 1 and 1 : 8, respectively). (D) Proposed mechanism for the formation of the nanotadpoles during the solution phase step involving seeded growth. Here, the reduction of AuCl by citrate leads to the formation of small Au nanocrystals (as denoted by the black arrows in B and D), that can assembly into 1D chains from the surface of the Au NPs seeds leading to the formation of the nanotadpoles.

and that the tails then grow at the surface of these seeds by imperfect oriented attachment (nonclassical growth) in the second, solution phase step (Fig. 5D). This agrees with previous reports in which it Au NPs with diameters below 10 nm in size can assemble into 1D morphologies by dipole–dipole and van der Waals interactions in the presence of citrate.[15]

The utilization of water as the solvent (Fig. S6, ESI†) and citrate (Fig. S7, ESI†) was fundamental for the formation of the tadpoles. Specifically, only irregular NPs were observed when the solvent employed during the solution-phase step was changed to methanol, ethanol, or isopropanol (Fig. S6, ESI†). This may be related to the lower solubility of citrate and AuCl in these solvents. Similarly, no tadpoles were formed when the utilization of citrate was replaced by sodium borohydride, ascorbic acid, or hydroquinone. This indicates that citrate reduction during the solution-phase step may be essential to form numerous small Au nanocrystals by self-nucleation from AuCl which then assemble to form 1D chains attached to the Au NPs seeds obtained in the first step (Fig. S7, ESI†). Our results indicate that both the mechanochemical and solution phase steps are important for the formation of the Au nanotadpoles. The key parameters that can be identified as crucial for the synthesis of nanotadpoles by the mechano-colloidal method are: ball milling under moderate conditions so that the metal precursor is not completely consumed, use of a solvent in which the starting materials can have their solubilization facilitated, and use of reducing agent and stabilizers during the solution phase step that enable to maneuver nucleation and growth stages to yield the desired NP morphology. We have also applied the mechano-colloidal approach to the synthesis of Ag NPs under similar conditions as described for Au (Fig. S8, ESI†). Although some NPs with elongated shapes could be observed, the formation of tadpoles was not detected. Therefore, the application of the mechano-colloidal approach to other metal NPs requires further optimizations on the choice of reducing and stabilizing agents to allow for shape control.

In conclusion, we described a mechano-colloidal approach for the synthesis of controlled metal NPs that can marry the attractive features of both mechanochemistry and solution-phase synthesis. By employing Au as a proof-of-concept example, Au nanotadpoles could be obtained from a solid mixture containing AuCl, citrate, and PVP at room temperature. The first step involving ball-milling is employed to generate NPs seeds. Then, in a second solution-phase step, the solid reaction mixture containing the NPs seeds and the unreacted metal precursor is dispersed in a solvent such as water. In the synthesis of the nanotadpoles, the mechanochemical step led to the formation of spherical NPs seeds, and the solution phase step enabled the generation of small Au nanocrystals which could be assembled into 1D chains from the surface of the NPs seeds to generate the nanotadpole morphology. The nanotadpoles may find applications in areas such as catalysis, self-assembly, surface-enhanced Raman scattering, sensing, and the development of nanomotors. We envision that the proposed mechano-colloidal approach can be extended and optimized to other metal NPs shapes and compositions. It can also be adapted to the synthesis of multimetallic NPs by employing mixtures of precursors or by introducing other precursors and reagents during the solution phase step.

This work was supported by FAPESP (Grant 2015/26308-7) and the Serrapilheira Institute (Grant Serra-1709-16900). JQ and PFMO thank FAPESP for the fellowships (Grants 2016/17866-9 and 2017/15456-0). We thank the Brazilian Synchrotron Light Laboratory (LNLS, CNPEM) for XAS (XAFS2) analysis. DCO thanks CNPq for the research fellowship (Bolsista do CNPq – Brasil, 305340/2017-4).

Conflicts of interest

There are no conflicts to declare.

Notes and references

1 T. S. Rodrigues, A. G. M. Da Silva and P. H. C. Camargo, *J. Mater. Chem. A*, 2019, **7**, 5857–5874.
2 (*a*) Y. Xia, Y. Xiong, B. Lim and S. E. Skrabalak, *Angew. Chem., Int. Ed.*, 2009, **48**, 60–103; (*b*) Z. Wu, S. Yang and W. Wu, *Nanoscale*, 2016, **8**, 1237–1259.
3 F. Fiévet, S. Ammar-Merah, R. Brayner, F. Chau, M. Giraud, F. Mammeri, J. Peron, J. Y. Piquemal, L. Sicard and G. Viau, *Chem. Soc. Rev.*, 2018, **47**, 5187–5233.
4 (*a*) M. J. Rak, T. Friščić and A. Moores, *Faraday Discuss.*, 2014, **170**, 155–167; (*b*) M. J. Rak, T. Friščić and A. Moores, *RSC Adv.*, 2016, **6**, 58365–58370; (*c*) M. J. Rak, N. K. Saadé, T. Friščić and A. Moores, *Green Chem.*, 2014, **16**, 86–89; (*d*) D. Debnath, C. Kim, S. H. Kim and K. E. Geckeler, *Macromol. Rapid Commun.*, 2010, **31**, 549–553; (*e*) D. Debnath, S. H. Kim and K. E. Geckeler, *J. Mater. Chem.*, 2009, **19**, 8810; (*f*) T. Premkumar and K. E. Geckeler, *Colloids Surf., A*, 2014, **456**, 49–54; (*g*) X. Li, Z. Zhang, W. Xiao, S. Deng, C. Chen and N. Zhang, *J. Mater. Chem. A*, 2019, **7**, 14504–14509; (*h*) E. Zhang, G.-P. Hao, M. E. Casco, V. Bon, S. Grätz and L. Borchardt, *J. Mater. Chem. A*, 2018, **6**, 859–865.
5 J. L. Howard, Q. Cao and D. L. Browne, *Chem. Sci.*, 2018, **9**, 3080–3094.
6 (*a*) Y. Xia, K. D. Gilroy, H.-C. Peng and X. Xia, *Angew. Chem., Int. Ed.*, 2017, **56**, 60–95; (*b*) C. Xu, S. De, A. M. Balu, M. Ojeda and R. Luque, *Chem. Commun.*, 2015, **51**, 6698–6713; (*c*) P. Baláž, in *Mechanochemistry in Nanoscience and Minerals Engineering*, ed. P. Baláž, Springer Berlin Heidelberg, Berlin, Heidelberg, 2008, pp. 1–102.
7 S. Grazulis, D. Chateigner, R. T. Downs, A. F. T. Yokochi, M. Quiros, L. Lutterotti, E. Manakova, J. Butkus, P. Moeck and A. Le Bail, *J. Appl. Crystallogr.*, 2009, **42**, 726–729.
8 R. L. Penn, *Science*, 1998, **281**, 969–971.
9 T. Friščić, I. Halasz, P. J. Beldon, A. M. Belenguer, F. Adams, S. A. J. Kimber, V. Honkimäki and R. E. Dinnebier, *Nat. Chem.*, 2013, **5**, 66–73.
10 L. M. Liz-Marzán, M. Giersig and P. Mulvaney, *Langmuir*, 1996, **12**, 4329–4335.
11 (*a*) P. Dash, T. Bond, C. Fowler, W. Hou, N. Coombs and R. W. J. Scott, *J. Phys. Chem. C*, 2009, **113**, 12719–12730; (*b*) A. Villa, N. Dimitratos, C. E. Chan-Thaw, C. Hammond, G. M. Veith, D. Wang, M. Manzoli, L. Prati and G. J. Hutchings, *Chem. Soc. Rev.*, 2016, **45**, 4953–4994.
12 X. Lu, H.-Y. Tuan, B. A. Korgel and Y. Xia, *Chem. – Eur. J.*, 2008, **14**, 1584–1591.
13 M. F. Lengke, B. Ravel, M. E. Fleet, G. Wanger, R. A. Gordon and G. Southam, *Environ. Sci. Technol.*, 2006, **40**, 6304–6309.
14 (*a*) L. Huang, M. Wang, Y. Zhang, Z. Guo, J. Sun and N. Gu, *J. Phys. Chem. C*, 2007, **111**, 16154–16160; (*b*) A. G. M. da Silva, E. A. Lewis, T. S. Rodrigues, T. J. A. Slater, R. S. Alves, S. J. Haigh and P. H. C. Camargo, *Chem. – Eur. J.*, 2015, **21**, 12314–12320.
15 (*a*) B. Jin, M. L. Sushko, Z. Liu, C. Jin and R. Tang, *Nano Lett.*, 2018, **18**, 6551–6556; (*b*) Y. Liu, X.-M. Lin, Y. Sun and T. Rajh, *J. Am. Chem. Soc.*, 2013, **135**, 3764–3767; (*c*) C. Zhu, S. Liang, E. Song, Y. Zhou, W. Wang, F. Shan, Y. Shi, C. Hao, K. Yin, T. Zhang, J. Liu, H. Zheng and L. Sun, *Nat. Commun.*, 2018, **9**, 421.

